



Mass spectrometry imaging of phosphatidylcholine metabolism in lungs administered with therapeutic surfactants and isotopic tracers

Shane R. Ellis^{1,2,3,*}, Emily Hall⁴, Madhuriben Panchal^{4,5}, Bryn Flinders¹, Jens Madsen⁶, Grietof Koster^{4,5}, Ron. M. A. Heeren¹, Howard W. Clark^{6,7}, and Anthony D. Postle^{4,5,*}

¹Division of Imaging Mass Spectrometry, Maastricht MultiModal Molecular Imaging (M4I) Institute, Maastricht University, Maastricht, The Netherlands; ²Molecular Horizons and School of Chemistry and Molecular Bioscience, University of Wollongong, Wollongong, New South Wales, Australia; ³Illawarra Health and Medical Research Institute, Wollongong, NSW, Australia; ⁴Academic Unit of Clinical & Experimental Sciences, Faculty of Medicine, University of Southampton, Southampton, United Kingdom; ⁵National Institute for Health Research Southampton Biomedical Research Centre, University Hospital Southampton, Southampton, United Kingdom; ⁶Elizabeth Garrett Anderson Institute for Women's Health, Faculty of Population Health Sciences, University College London, London, United Kingdom; and ⁷National Institute for Health Biomedical Research Centre, University College London Hospital Biomedical Research Centre, London, United Kingdom

Abstract Mass spectrometry imaging (MSI) visualizes molecular distributions throughout tissues but is blind to dynamic metabolic processes. Here, MSI with high mass resolution together with multiple stable isotope labeling provided spatial analyses of phosphatidylcholine (PC) metabolism in mouse lungs. Dysregulated surfactant metabolism is central to many respiratory diseases. Metabolism and turnover of therapeutic pulmonary surfactants were imaged from distributions of intact and metabolic products of an added tracer, universally ¹³C-labeled dipalmitoyl PC (U¹³C-DPPC). The parenchymal distributions of newly synthesized PC species were also imaged from incorporations of *methyl-D₉*-choline. This dual labeling strategy demonstrated both lack of inhibition of endogenous PC synthesis by exogenous surfactant and location of acyl chain remodeling processes acting on the U¹³C-DPPC-labeled surfactant, leading to formation of polyunsaturated PC lipids. This ability to visualize discrete metabolic events will greatly enhance our understanding of lipid metabolism in diverse tissues and has potential application to both clinical and experimental studies.

Supplementary key words Pulmonary surfactant • lipids • isotope labeling • matrix-assisted laser desorption/ionization • remodeling

Phospholipids represent the major surface-active components of lung surfactant. The phospholipid

content of surfactant contains high levels of the disaturated species dipalmitoyl phosphatidylcholine (DPPC; PC16:0/16:0) that is maintained by a complex intralveolar metabolism. Unsaturated PC lipids synthesized on the endoplasmic reticulum are subject to acyl remodeling catalyzed by sequential phospholipase A₂ and lysoPC acyltransferase activities (1, 2), intracellular trafficking into lamellar body storage vesicles, and secretion into the alveolus to form the mature DPPC-enriched surfactant. Surfactant enriched in DPPC is then secreted into the alveolar lining fluid by exocytosis of lamellar bodies, followed by rapid adsorption to the air:liquid interface. Surfactant is subsequently catabolized by alveolar epithelial type II (ATII) cell endocytosis (3), metabolism by alveolar macrophages (4) and loss up the bronchial tree (5). A proportion of the surfactant taken up by ATII cells is subsequently recycled into lamellar bodies for re-secretion into the alveolus (6, 7).

Prior work by some of us used the incorporation of deuterated *methyl-D₉*-choline into PC molecular species to probe surfactant metabolism in greater detail from biological extracts (8, 9). This work characterized the mechanisms of acyl remodeling in surfactant PC synthesis by animal models (9), adult volunteers (10) and acute respiratory disease syndrome patients (11). Recently, an alternative acyl remodeling mechanism involved in surfactant metabolism was demonstrated, whereby a proportion of surfactant DPPC is selectively remodeled into PC species containing the polyunsaturated fatty acids arachidonate (20:4) and docosahexaenoate (22:6) (12). This study administered exogenous therapeutic surfactants to adult mice, with tracer amounts of the universally ¹³C-labeled (U¹³C) isotopomer of DPPC (U¹³C-DPPC) added to the surfactant.

This article contains [supplemental data](#).

*For correspondence: Shane R. Ellis, sellis@uow.edu.au; Anthony D. Postle, A.D.Postle@soton.ac.uk.

Current address for Bryn Flinders: Hair Diagnostix, Dutch Screening Group, Gaetano Martinolaan 63A, 6229 GS Maastricht, The Netherlands.



In addition to quantifying overall surfactant catabolism, this experimental approach enabled characterization of recycling mechanisms of surfactant DPPC by following the incorporations into intact PC species of $U^{13}C$ -labeled fragments derived from $U^{13}C$ -DPPC hydrolysis.

Lung surfactant components such as DPPC can also be analyzed by mass spectrometry imaging (MSI), which offers a powerful approach to study the distributions of lipids throughout biological tissues (13, 14). MALDI-MSI has demonstrated enriched location of polyunsaturated PC species within the bronchial tree (15), a distribution potentially linked to the involvement of oxidation products of arachidonate in the pathology of inflammatory lung diseases (16, 17). However, the location of synthesis within lung tissue of PUFA-containing PC species, both directly by the CDP:choline pathway and by acyl remodeling, has not been established. This information is lacking because conventional MSI is only capable of providing static lipid compositions within a given tissue region at a fixed moment in time. This static limitation can be overcome by coupling MSI with stable isotope labeling: isotope uptake into lipid metabolic processes can be detected in a time-resolved manner, reflected by measurements of mass-shifted lipid signals containing the isotopic tracer or the products of its metabolic conversion. Such approaches have been more widely applied using secondary ion mass spectrometry (SIMS), but because of the extensive fragmentation observed by SIMS whereby often only elemental or diatomic fragments are observed (e.g., Nano SIMS), it is difficult to study the metabolism of individual lipid species (18, 19). Recently, several groups have coupled isotope labeling with MALDI (20) or with desorption electrospray ionization (21), both of which enable detection of intact lipid species. These studies utilized heavy water labeling of mice to study region-specific lipid synthesis in breast cancer and mouse brain tissue, respectively. The widespread and nonspecific nature of heavy water labeling were significant limitations of these studies. These limitations, together with the modest mass resolving power of the MSI instrumentation used, meant many lipid signals, representing combinations of different labeled and unlabeled species, and different metabolic processes remained unresolved.

Here, we used MALDI-MSI at high mass resolving power coupled to a dual labeling approach utilizing both *methyl*- D_9 choline chloride and $U^{13}C$ -DPPC administered to mice to visualize lung and surfactant lipid metabolism. We report the simultaneous characterization and visualization of surfactant PC synthesis and catabolism throughout the lung tissue.

MATERIALS AND METHODS

Preparation of labeled surfactants

$U^{13}C$ -DPPC was mixed with the porcine-derived Poractant alfa and the synthetic CHF5633 surfactants as described

previously (12). Isotopic enrichments of $U^{13}C$ -DPPC in Poractant alfa and in CHF5633 were, respectively, 7.55% and 2.87% of total DPPC.

Animal labeling and sample preparation procedure

Mouse lungs used in this study were provided from a previous study of exogenous surfactant turnover in mice (12). Tissues were stored at $-80^{\circ}C$, shipped on dry ice for MALDI-MSI, then stored at $-80^{\circ}C$ until sectioning and analysis. Briefly, animal procedures were approved internally by the University of Southampton Animal Welfare and Ethical Review Body and externally by the Home Office, Animals in Science Regulation Unit. Wild-type (C57BL/6) male mice aged between 8 and 12 weeks were used for this study. Randomization was not relevant in this study. Similarly, blinding was not practicable as the two surfactant used had different phospholipid compositions. Each mouse was instilled intranasally with 50 μ l (4 mg, equivalent to 200 mg/kg body weight) of either Poractant alfa or the synthetic surfactant CHF5633, both containing $U^{13}C$ -DPPC. At the same time, each mouse also received a 100 μ l intraperitoneal injection of *methyl*- D_9 -choline chloride (10 mg/ml in water). After labeling, the mice were euthanized by carbon dioxide asphyxia at 6, 12, 18, or 24 h. Bronchoalveolar lavage was performed in situ with 4×0.9 ml PBS, and the recovered bronchoalveolar lavage fluid (BALF) aliquots were combined. BALF was centrifuged at $300 \times g$ for 10 min at $4^{\circ}C$ to pellet cells, and the supernatants were then transferred to new vials and stored at $-80^{\circ}C$ until extraction. Lung parenchyma was quickly dissected from the main bronchi, placed in cryotubes and snap-frozen in liquid nitrogen. Further details are provided in reference (12).

Alveolar macrophage labeling in vivo

For in vivo labeling studies, eight male wild-type C57BL6 mice were instilled with CHF5633 surfactant containing $U^{13}C$ -DPPC, then injected with *methyl*- D_9 -choline chloride 18 h later. After 3 h, mice were euthanized and BALF obtained, from which alveolar macrophages were isolated by centrifugation at $400g$ for 10 min. BALF Macrophages were purified by adherence to plastic tissue-culture dishes and were subsequently washed three times with 0.9% saline to remove adherent surfactant.

Macrophage phospholipid analysis

Total lipids were extracted by scraping adherent alveolar macrophages into 800 μ l of 0.9% saline after adding dimyristoyl PC (10 nmoles) as internal standard, followed by extraction with dichloromethane (2 ml), methanol (2 ml), and water (1 ml) (22). After mixing and centrifugation at $1,500g$, $20^{\circ}C$ for 10 min, the dichloromethane-rich lower phase was recovered, dried under a stream of nitrogen gas, and stored at $-20^{\circ}C$ until analysis by mass spectrometry. Mass spectrometry analysis was performed on a Waters XEVO TQ mass spectrometer (Waters UK, Elstree, UK) using electrospray ionization as described previously (9). Unlabeled PC and newly synthesized PC labeled with D_9 -choline were detected using precursor ion scans of the PC headgroup fragment ions at $m/z +184$ and $m/z +193$, respectively. Precursor ion scans of $m/z +189$ detected the PC species containing five labeled ^{13}C atoms in their phosphocholine head group.

Tissue preparation for MALDI-MSI

Frozen lung tissue was sectioned for MALDI-MSI analysis using a Leica CM 1860 UV cryomicrotome (Leica Microsystems, Wetzlar, Germany) at a temperature of -20°C to produce 12 μm -thick tissue sections, which were thaw mounted onto clean indium tin oxide-coated glass slides (Delta Technologies, Loveland, CO). Tissue sections were stored at -80°C until matrix application and analysis. 2,5-dihydroxybenzoic acid was prepared as a 20 mg/mL solution in 2:1 CHCl_3 :MeOH (v/v) and applied to the sample using a SunCollect automatic pneumatic sprayer (Sunchrom GmbH, Friedrichsdorf, Germany). In total 15 layers of matrix were deposited onto the tissue. The first three layers were deposited using a flow rate of 10, 20, and 30 $\mu\text{L}/\text{min}$, respectively, and all subsequent layers at 40 $\mu\text{L}/\text{min}$.

Hematoxylin and eosin staining

Hematoxylin and eosin staining was performed on tissue sections after MSI analysis. The matrix was removed by immersion in 100% methanol for 30 s, after which the following protocol was used. The tissues were first washed with series of solutions ($2 \times 95\%$ EtOH, $2 \times 70\%$ EtOH and deionized water for 2 min each), stained with hematoxylin for 3 min and subsequently washed with running tap water for 3 min. Tissues were then stained with eosin for 30 s and washed with running tap water for 3 min. After staining, the samples were placed into 100% ethanol for 1 min, then in xylene for 30 s. Finally, glass coverslips were placed onto the samples using Entellen mounting medium. High-resolution optical scans of the stained tissue sections were acquired using a Leica Aperio CS2 (Leica Biosystems Imaging, Vista, CA).

MALDI-MSI

MALDI-MSI was performed using a hybrid Orbitrap Elite mass spectrometer (Thermo Fisher Scientific GmbH, Bremen, Germany) coupled to a reduced pressure ESI/MALDI ion source (Spectrograph LLC, Kennewick, WA). Further details on the experimental setup can be found in reference (23). All MSI data were collected using a nominal mass resolution setting of 240,000 @ m/z 400, an m/z range of 350–1,000 and a pixel size of $40 \times 40 \mu\text{m}^2$. Tandem mass spectrometry (MS/MS) was performed on MALDI ions generated directly from lung tissue sections to confirm the identification the selected signals. MS/MS spectra were acquired using resonant collision-induced dissociation, a ± 0.5 Da isolation window and Orbitrap detection of fragments.

Data analysis

MSI data analysis and visualization were performed using LipostarMSI (Molecular Horizon Srl, Perugia, Italy) (24). During data import, mass spectra were recalibrated using the $[\text{PC32:0}+\text{Na}]^+$ ion as a lock mass (theoretical $m/z = 756.551374$). Peak picking was performed using a relative intensity threshold of 0.05%, a minimum peak frequency of 0.5%, and an m/z alignment tolerance of 3 ppm. All MSI data visualizations were generated using total ion current normalization with hotspot removal (quantile thresholding, high quantile = 99%). An exception was the ratio images that were produced by normalization to the denominator ion signal ($[\text{PC32:0}+\text{Na}]^+$ or $[\text{PC32:1}+\text{Na}]^+$).

Xcalibur QualBrowser (version 4.1.50, Thermo Fisher Scientific GmbH, Bremen, Germany) and Python 3.7.6 together with the pymzreader 1.0.1 ([pymzreader/\), NumPy and Matplotlib libraries were used for analysis and visualization of .raw MS and MS/MS data spectral data.](https://pypi.org/project/</p></div><div data-bbox=)

Lipid nomenclature

Sum-composition PC molecular species are generally denoted by the number of total fatty acyl carbon atoms followed by the number of unsaturated double bonds. For example, PC36:4 corresponds to a PC lipid with 36 carbons and 4 double bonds distributed across the two acyl chains. In cases where the length and degree of unsaturation of each acyl chain are known, but the *sn*-positioning of individual fatty acyls is undefined, the underscore nomenclature is used, for example PC16:0_20:4. When the *sn*-positioning is defined, the “/” nomenclature is used. For example, PC16:0/20:4 corresponds to a PC lipid with a 16:0 acyl chain at the *sn*-1 position and a 20:4 acyl chain at the *sn*-2 position. Stereochemistry and double bond positions are undefined. Sum-composition lipid species can consist of multiple molecular species. For instance, PC36:4 could be either PC18:2_18:2 or PC16:0_20:4. The exception is for newly synthesized PC species containing $^{13}\text{C}_{24}$ -palmitoyl-lysoPC derived from U^{13}C -DPPC metabolism where, for instance, $^{13}\text{C}_{24}$ -PC36:4 is unambiguously the palmitoylarachidonoyl PC16:0_20:4 species. Fragment ion nomenclature is based on that proposed by Pauling *et al.* in reference (25).

RESULTS

MSI of isotopically labeled lipids

We aimed to analyze lipid metabolism in mouse lung tissue after dosing intraperitoneally with D_9 -choline chloride and intranasally with an exogenous therapeutic surfactant containing U^{13}C -DPPC. Both the complex mass spectra generated by MALDI analysis of biological tissue and the expected low abundance of labeled lipid species (~ 1 –2% relative to the corresponding unlabeled lipid species) make the unambiguous detection of both D_9 -choline-labeled PC and U^{13}C -DPPC directly from lung tissue a challenge. Here, we have utilized the high resolving power of an Orbitrap mass spectrometer to enable unambiguous detection of isotopically labeled species in the presence of isobaric interferences arising from endogenous lipids. The average mass spectrum of a mouse lung tissue showed that protonated, sodiated, and potassiated ions of PC lipids dominate the spectrum with PC32:0 (predominately PC16:0/16:0), the major lipid component of lung surfactant, providing the highest signal intensities with the base peak at m/z 756.5513 assigned as the $[\text{PC32:0}+\text{Na}]^+$ ion (Fig. 1A). Importantly, we detected D_9 -labeled PC32:0, corresponding to PC32:0 synthesized over the 12 h between label injection and sacrifice, with the $[\text{D}_9\text{-PC32:0}+\text{Na}]^+$ ion detected at m/z 765.6079 with an intensity of $\sim 1\%$ compared with the unlabeled variant (Fig. 1B). The corresponding protonated and potassiated ions were also observed (supplemental Fig. S1). We detected $[\text{U}^{13}\text{C-PC32:0}+\text{Na}]^+$ at m/z 796.6854 that arises exclusively from the therapeutic

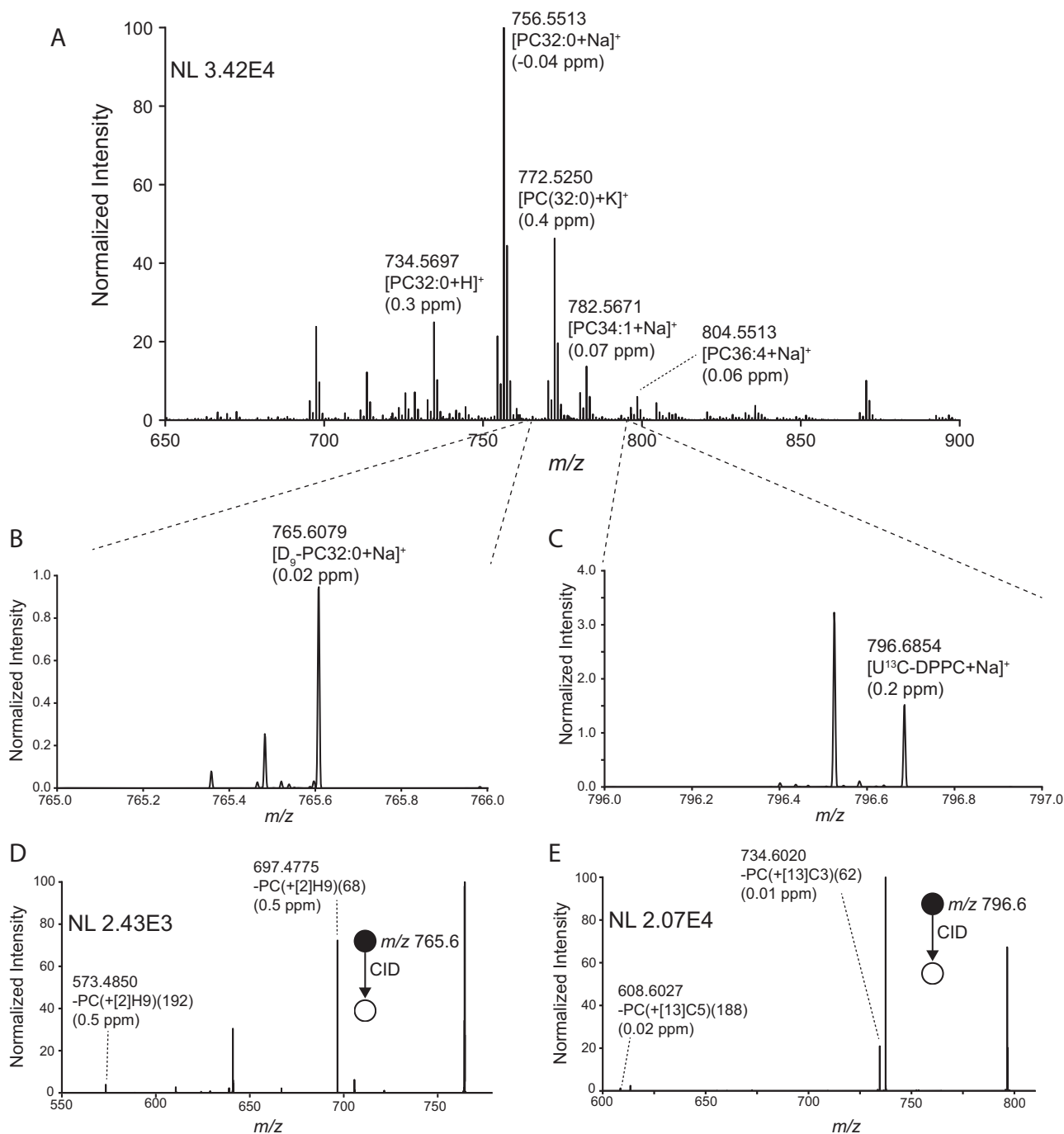


Fig. 1. A: Averaged positive-ion MALDI spectrum of mouse lung tissue administered with D₉-choline and U¹³C-DPPC-containing CHF5633 surfactant 12 h before tissue collection. Lipid identifications and parts-per-million (ppm) mass errors for several abundant lipid species are indicated. B, C: Zoom-in of the spectrum in (A) at the *m/z* 765–766 range (B) demonstrating the detection of [D₉-PC32:0+Na]⁺ and at the *m/z* 796–797 range (C) demonstrating the detection of [U¹³C-DPPC+Na]⁺. D, E: MS/MS spectra for precursor ions at (D) *m/z* 765.5 ± 0.5 and *m/z* 796.6 ± 0.5 corresponding to [D₉-PC32:0+Na]⁺ and [U¹³C-DPPC+Na]⁺, respectively, with supporting fragments annotated. Additional peaks in the MS/MS spectra arise from the co-isolation and fragmentation of isobaric ions. DPPC = PC16:0/16:0. MS/MS, tandem mass spectrometry; PC, phosphatidylcholine; U¹³C-DPPC, universally ¹³C-labeled dipalmitoyl PC.

surfactant (Fig. 1C), as well as its corresponding protonated and potassiumated ions (supplemental Fig. S2). Identification of both labeled PC species ions was further corroborated by MS/MS with specific fragments consistent with the expected

deuterium ([D₉-PC32:0+Na]⁺, Fig. 1D) and ¹³C ([U¹³C-PC32:0+Na]⁺, Fig. 1E) labeling patterns detected with high mass accuracy (< 1 ppm mass error). These results confirm the ability to detect both newly synthesized PC lipids via the Kennedy

pathway and D₉-choline incorporation as well as exogenous surfactant using U¹³C-PC32:0 as a specific marker ion directly from lung tissue sections using MALDI-MSI.

IMAGING OF SURFACTANT PHOSPHATIDYLCHOLINE METABOLISM IN MOUSE LUNGS

Next, we sought to study the distribution of both D₉-choline-labeled PC32:0 and intranasally dosed exogenous surfactant within mice lung tissue. We administered two different surfactants—synthetic CHF5633 and porcine lung-derived Poractant alfa. These preparations have different phospholipids, with CHF5633 being composed of a 50/50 mixture of PC16:0/16:0 and PG16:0/18:1 while Poractant alfa contains the full complement of surfactant lipids. U¹³C-PC16:0/16:0 was added to both surfactants to monitor exogenous surfactant metabolism before intranasal administration to mice that were also injected with *methyl*-D₉-choline chloride to assess endogenous lung PC synthesis occurring via the Kennedy pathway (26).

CHF5633 synthetic surfactant

The distribution of several sodiated PC lipid ions throughout the mouse lung 12 h after administration of CHF5633 are shown in Fig. 2. The optical image of the hematoxylin and eosin stained of the same tissue after MSI is shown in Fig. 2A. The U¹³C-DPPC ion at m/z [M+Na]⁺ 796.6855 was located in one parenchymal area but not within bronchioles, demonstrating one extreme example of the regional deposition (Fig. 2B). As expected, the distribution of unlabeled DPPC at m/z [M+Na]⁺ 756.5514 (Fig. 2C) partially mirrored that of U¹³C-DPPC (Fig. 2A) because of the excess amount of unlabeled DPPC in the CHF5633 surfactant. By contrast, the distribution of ion signals corresponding to the incorporation *methyl*-D₉-choline into PC32:0 via the Kennedy pathway (Fig. 2D; [M+Na]⁺, m/z 765.6079) exhibited a reduced intensity in regions where U¹³C-DPPC was highest, demonstrated by the ratio of D₉-PC32:0+Na⁺/PC32:0+Na⁺ (Fig. 2E); this observation could suggest inhibition of endogenous PC synthesis by the exogenous surfactant. However, both unlabeled PC32:1 (Fig. 2F, [M+Na]⁺, m/z 754.5359), which is an integral component of mouse lung surfactant but absent from CHF5633 and D₉-PC32:1 (Fig. 2G, [M+Na]⁺, m/z 763.5923) were similarly present at lower intensity in regions enriched in CHF5633. Consequently, the ratio of [D₉-PC32:1+Na]⁺/[PC32:1+Na]⁺ was more uniform across the lung parenchyma (Fig. 2H) with no decrease in areas of high U¹³C-DPPC signal. Similar distributions were apparent for other endogenous PC species with a parenchymal distribution (supplemental Fig. S3) and from tissue obtained from another mouse administered with both labels 6 h before tissue collection

(supplemental Fig. S4). These results suggest the decreased [D₉-PC32:0+Na]⁺/[PC32:0+Na]⁺ ratios are a consequence of the regional, nonspecific accumulation of the DPPC-rich CHF5633 surfactant, rather than inhibition of PC synthesis. This is supported by extracted region-specific spectra that show regions of high U¹³C-DPPC to contain 2–3 fold higher signal for unlabeled DPPC than surrounding regions (supplemental Fig. S5). Although some lipid signal was observed on the glass slide adjacent to the tissue sections, which may arise because of smearing artefacts during tissue mounting, this did not alter the on-tissue distributions.

In agreement with previous reports (15), MSI demonstrated spatial segregation of unlabeled PC species, with the polyunsaturated PC species PC36:4 (Fig. 3A, [M+Na]⁺, m/z 804.5514) and PC38:6 (Fig. 3B, [M+Na]⁺, m/z 828.5515) restricted to bronchiolar regions (Fig. 3C, D). Similar results were obtained from another animal euthanized 6 h after label administration (supplemental Fig. S6). Little to no signal was observed for exogenous CHF5633-specific U¹³C-DPPC in the bronchiolar regions. Unfortunately, because of the low abundance of these polyunsaturated species compared with PC32:0 and PC32:1 that form major lipid components of surfactant, combined with the presence of an unresolved isotopologue from another lipid-related ion, the corresponding D₉-containing PC36:4 and PC38:6 ions could not be unambiguously detected.

Incorporation of *methyl*-D₉-choline also facilitated analysis of the distribution patterns of other newly synthesized PC species. Other PC species characteristic of lung tissue rather than surfactant, such as PC34:1 and PC34:2 (27) were distributed more equally between bronchiolar and parenchymal regions both for unlabeled and D₉-choline-labeled species (supplemental Fig. S3). Similar distributions were observed for the same ions detected from lung collected from another mouse 6 h after label administration (supplemental Fig. S4). For all labeled ions discussed above, no signal was observed in a control lung tissue that was not administered with either D₉-choline or U¹³C-DPPC (supplemental Fig. S7).

Poractant alfa porcine surfactant

Nasal administration of the porcine-derived Poractant alfa surfactant typically achieved a more widespread distribution in the lungs compared with CHF5633, illustrated by the distribution of the [U¹³C-DPPC+Na]⁺ ion at 12 h postdosing (Fig. 4A). Analysis of another mouse 18 h after administration showed comparable results (supplemental Fig. S8). We observed a more uniform distribution of unlabeled [PC32:0+Na]⁺ (Fig. 4B) and [D₉-PC32:0+Na]⁺ (Fig. 4C, D), although the normalized signal intensity for [D₉-PC32:0+Na]⁺ was still slightly more intense in lung regions with a relatively low U¹³C-DPPC signal because of the presence of unlabeled PC32:0 in the Poractant alfa surfactant.

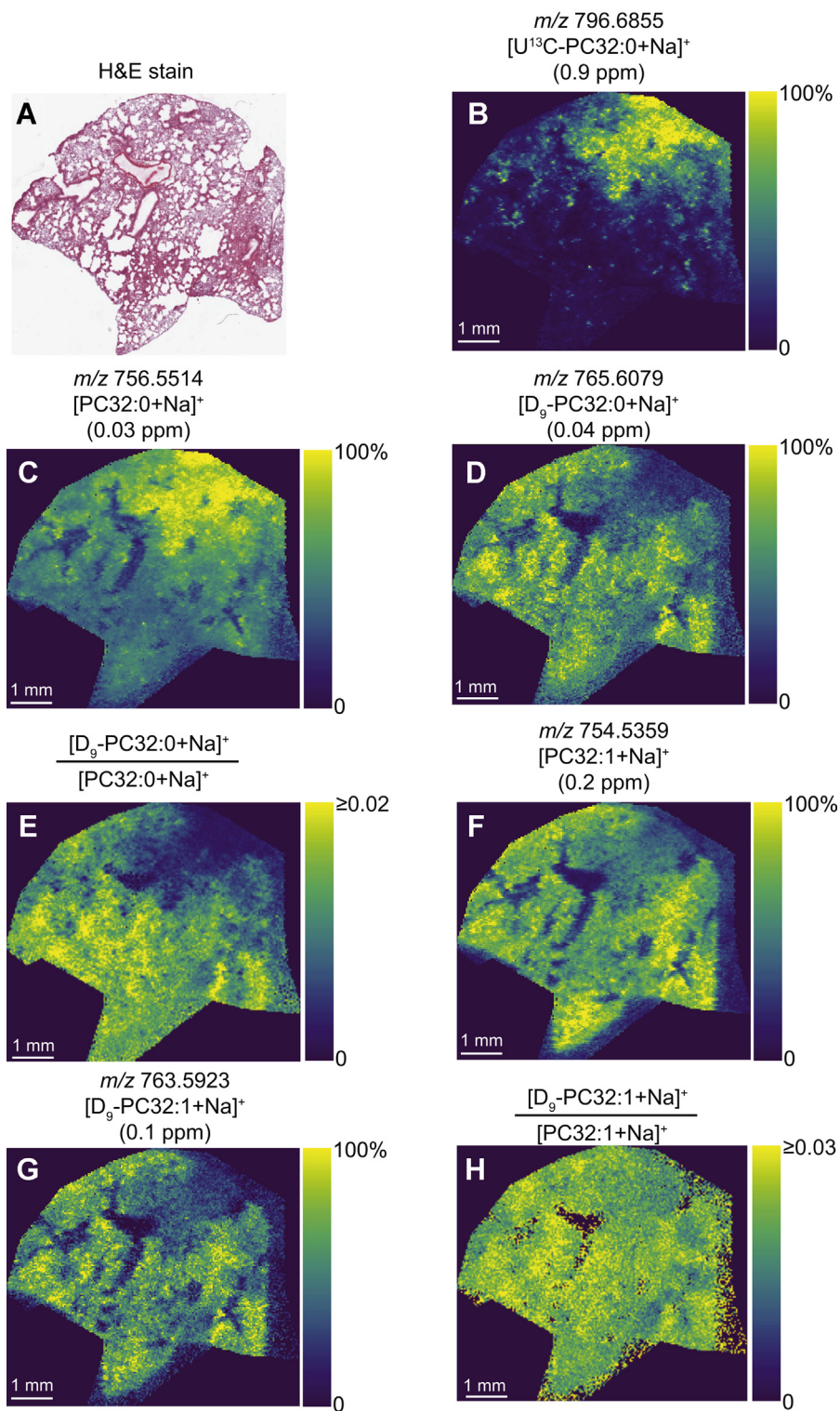


Fig. 2. MALDI-MSI data from the same mouse lung tissue analyzed in Fig. 1. A: Optical image of the post-MSI, H&E-stained tissue section. B–D, F–G: Ion images of (B) m/z 796.6855 ($[U^{13}C\text{-DPPC+Na}]^+$), (C) m/z 756.5514 ($[PC32:0+Na]^+$), (D) m/z 765.6079 ($[D_9\text{-PC32:0+Na}]^+$), (F) m/z 754.5359 ($[PC32:1+Na]^+$), and (G) m/z 763.5923 ($[D_9\text{-PC32:1+Na}]^+$). E, H: Ratio images of (E) $[D_9\text{-PC32:0+Na}]^+:[PC32:0+Na]^+$ and (H) $[D_9\text{-PC32:1+Na}]^+:[PC32:1+Na]^+$. Part-per-million (ppm) mass errors are indicated in parentheses. All images were visualized using total-ion-current normalization and using hotspot removal (high quantile = 99%). DPPC = PC16:0/16:0. $U^{13}C\text{-DPPC}$, universally ^{13}C -labeled dipalmitoyl PC; PC, phosphatidylcholine; MSI, mass spectrometry imaging; H&E, hematoxylin and eosin.

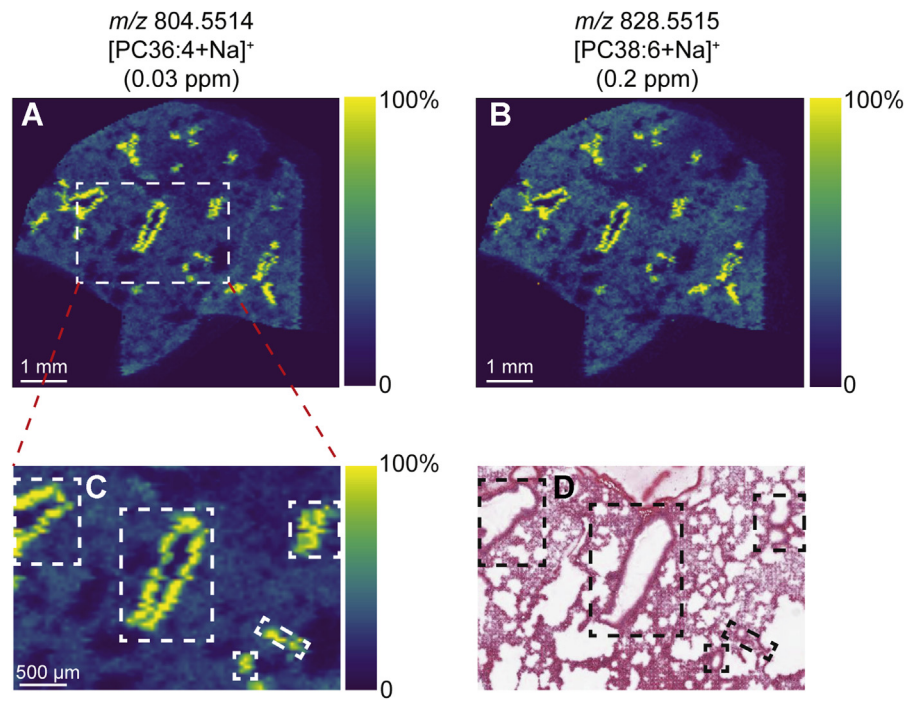


Fig. 3. MALDI-MSI data from the same mouse lung tissue analyzed in Fig. 1. Ion images of (A) m/z 804.5514 ($[PC_{36:4}+Na]^+$) and (B) m/z 828.5515 ($[PC_{38:6}+Na]^+$). C: Enlarged image of the region marked by the white box in (A) showing these polyunsaturated lipids localize to the bronchiolar regions, as identified by the post-MSI H&E-stained section (D). All images were visualized using total-ion-current normalization and using hotspot removal (high quantile = 99%). H&E, hematoxylin and eosin; MSI, mass spectrometry imaging.

Alveolar metabolism of $U^{13}C$ -DPPC-labeled surfactant in vivo

Previous analysis of the in vivo metabolism of $U^{13}C$ -DPPC-labeled surfactants in mice by shotgun lipidomics analysis of extracts identified the labeled $^{13}C_5$ -choline and $^{13}C_{24}$ -lysoPC16:0 moieties, generated by the respective phospholipase D and phospholipase A_1/A_2 enzymatic hydrolysis of $U^{13}C$ -DPPC, and their incorporation into PC molecular species (12). The molecular specificity for $^{13}C_5$ -PC lipid synthesis closely mirrored that observed for D_9 -choline labeling. This indicates that $^{13}C_5$ -choline generated by $U^{13}C$ -DPPC hydrolysis equilibrated with endogenous unlabeled choline and was then incorporated into PC by the CDP:choline (Kennedy) pathway (12). By contrast, reacylation of $^{13}C_{24}$ -LPC16:0 in both lung tissue and bronchoalveolar lavage was much more restricted, generating primarily only two polyunsaturated PC species, $^{13}C_{24}$ -PC16:0_{20:4} and $^{13}C_{24}$ -PC16:0_{22:6} (12). Our analysis of the lavage cell pellet from this study (12) showed a higher enrichment of both these species than in either lung tissue or bronchoalveolar lavage (supplemental Fig. S9). As this cell pellet contained both alveolar macrophages and the more easily precipitated lung surfactant, we hypothesized that reacylation of $^{13}C_{24}$ -LPC16:0 takes place in alveolar macrophages. To test this, mice received nasal administration of $U^{13}C$ -DPPC-labeled CHF5633, an intraperitoneal injection of methyl- D_9 -choline chloride (1 mg) 18 h later, were euthanized at 21 h after the first

administration, and lung tissue was taken for analysis. Alveolar macrophages were purified by centrifugation at 400g for 10 min, followed by differential adherence and washing to remove surfactant. There was negligible incorporation of the D_9 -choline label into alveolar macrophage PC, indicating a very low rate of PC synthesis de novo (data not shown). This contrasts strikingly with the high rate of surfactant PC synthesis by alveolar type II epithelial cells, which was greatest at 3 h (12). In comparison, active reacylation of $^{13}C_{24}$ -LPC16:0 via the Lands cycle (28, 29) by alveolar macrophages in vivo could be readily demonstrated 21 h after CHF5633 administration (12). Increased unlabeled PC32:0 in alveolar macrophages showed the uptake of exogenous surfactant by these cells (Fig. 5A). However, analysis of $^{13}C_{24}$ -PC also showed considerable metabolism of this intracellular exogenous surfactant over the same time period. The relative abundance of $U^{13}C$ -DPPC decreased from the initial administered value of 100% at 0 h, whereas those of $^{13}C_{24}$ -PC16:0_{20:4} and $^{13}C_{24}$ -PC16:0_{22:6} reacylation products increased (Fig. 5B). This finding was observed for all eight treated mice, with the mean relative abundances of $U^{13}C$ -DPPC, $^{13}C_{24}$ -PC16:0_{20:4}, and $^{13}C_{24}$ -PC16:0_{22:6} being $38.7 \pm 8.9\%$, $36.8 \pm 9.7\%$, and $24.5 \pm 6.4\%$ (mean \pm SD), respectively, relative to $U^{13}C$ -DPPC at $t=0$ (data not shown). There was no detectable synthesis of $^{13}C_{24}$ -DPPC by alveolar macrophages in vivo, which is consistent with the absence of DPPC synthesis by acyl remodeling in this cell type (30).

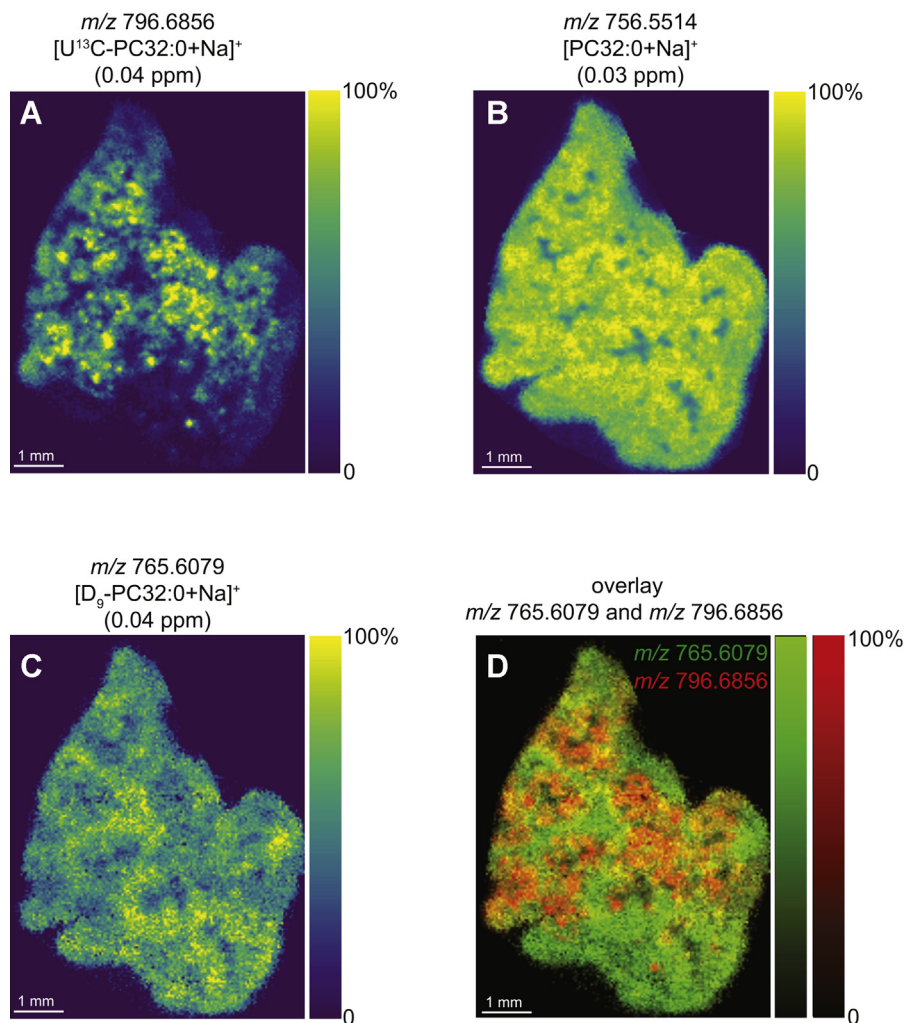


Fig. 4. MALDI-MSI data of mouse lung tissue after administration with D₉-choline and U¹³C-DPPC-containing Poractant alfa surfactant (labels administered 12 h prior to tissue collection). Ion images of (A) m/z 796.6856 ([U¹³C-DPPC+Na]⁺), (B) m/z 756.5154 [PC32:0+Na]⁺, and (C) m/z 765.6079 ([D₉-PC32:0+Na]⁺). D: Overlay image of [U¹³C-PC32:0+Na]⁺ (red) and [D₉-PC32:0+Na]⁺ (green). Part-per-million (ppm) mass errors are indicated in parentheses. All images were visualized using total-ion-current normalization and using hotspot removal (high quantile = 99%). DPPC = PC16:0/16:0. MSI, mass spectrometry imaging; PC, phosphatidylcholine; U¹³C-DPPC, universally ¹³C-labeled dipalmitoyl PC.

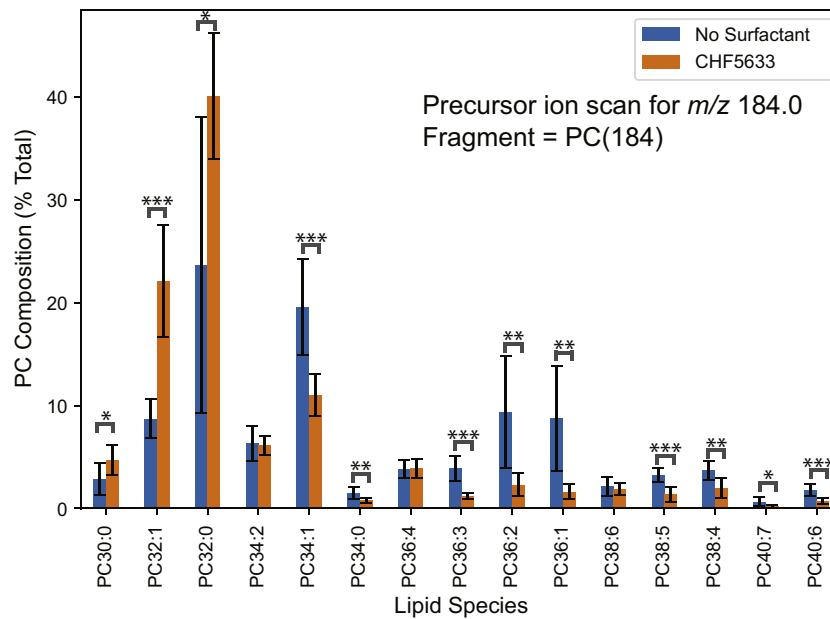
Imaging surfactant acyl remodeling in vivo

If re-acylation of ¹³C₂₄-LPC16:0 is restricted to alveolar macrophages in vivo, then ¹³C₂₄-PC16:0_20:4 should not co-localize with unlabeled PC36:4 in the bronchioles. Consequently, we monitored the distribution of ¹³C₂₄ PC species in mouse lungs 12 and 18 h after administration of U¹³C-DPPC-labeled Poractant alfa, specifically chosen for this analysis rather than CHF5633 for two reasons. First, the more uniform distribution of the porcine surfactant (Fig. 4) facilitated a clearer analysis of the distribution of surfactant metabolites. Second, enrichment of U¹³C-DPPC was higher in administered Poractant alfa than in CHF5633 (12), thereby providing sufficient signal intensity for imaging of the low abundance ¹³C₂₄-labeled acyl chain remodeling products.

In our MALDI-MSI analysis, we detected the [¹³C₂₄-PC16:0_20:4+Na]⁺ ion at m/z 828.6321 (Fig. 6A) with a

relative intensity of ~0.1% compared with the [DPPC+Na]⁺ ion in the mean spectrum. This compound could be assigned with high confidence because of the low mass error of 0.2 ppm and absence of this signal in an undosed mouse lung, despite its low abundance (supplemental Fig. S7). Further confirmation for the assignment of this ion as [¹³C₂₄-PC16:0_20:4+Na]⁺ was provided by the MS/MS spectrum (Fig. 6B) that revealed fragment ions at m/z 766.5479 and 640.5487, corresponding to the neutral losses of N(¹³CH₃)₃ (-PC(+[¹³C]3(62), -0.6 ppm mass error) and ¹³C₅H₁₅NO₄P (-PC(+[¹³C]5(188), -0.6 ppm mass error). These fragment ions are unambiguously attributable to a ¹³C-labeled phosphocholine headgroup. Unlabeled [PC36:4+Na]⁺ (green) was observed primarily in the bronchioles of mouse lungs at 12 h (Fig. 6C) and 18 h (Fig. 6D), along with a corresponding distribution of [U¹³C-DPPC+Na]⁺ (blue) and [¹³C₂₄-PC16:0_20:4+Na]⁺

A Alveolar macrophage lipid extract (unlabeled PC species)



B $^{13}\text{C}_{24}$ -labeled PC species

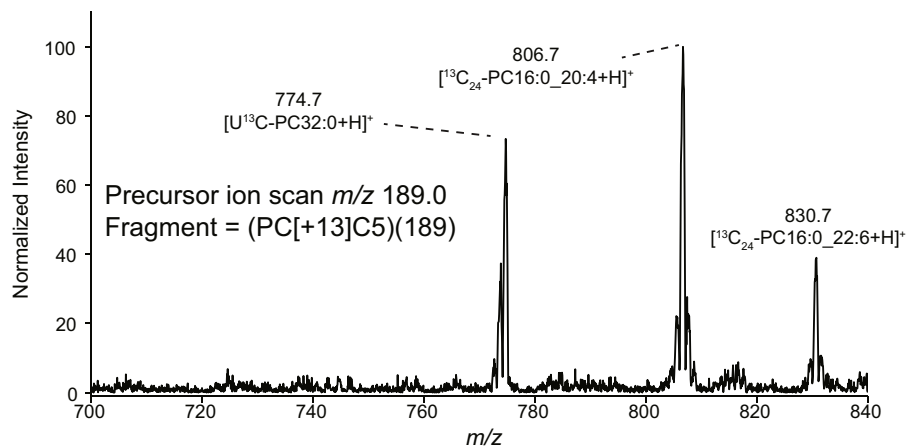


Fig. 5. Alveolar macrophage metabolism of labeled exogenous surfactant. U^{13}C -DPPC-labeled CHF5633 surfactant (4 mg in 50 μl) was administered intranasally to mice, followed 18 h later by an intraperitoneal injection with *methyl*- D_9 -choline chloride (1 mg). Mice were euthanized 3 h later, their lungs were lavaged and alveolar macrophages isolated by differential adherence. After washing with saline, macrophage lipids were extracted and analyzed by ESI-MS/MS. A: Unlabeled PC lipid composition of isolated alveolar macrophages using a precursor ion scan of m/z 184.0. Orange bars correspond to mice administered with CHF5633 surfactant and blue bars mice not administered with any exogenous surfactant. B: Precursor ions scan for m/z 189.0 for detection of PC species containing the ^{13}C phosphocholine headgroup derived from U^{13}C -DPPC. Error bars correspond to ± 1 standard deviations ($n = 8$ per group). DPPC = PC16:0/16:0. * $P < 0.05$, ** $P < 0.01$, *** $P < 0.001$. Significance was calculated by a two-tailed Student's t -test. MS/MS, tandem mass spectrometry; PC, phosphatidylcholine; U^{13}C -DPPC, universally ^{13}C -labeled dipalmitoyl PC.

(red) that is synthesized by successive de-acylation/re-acylation processes of U^{13}C -DPPC through the Lands cycle. These processes led to replacement of a U^{13}C -16:0 fatty acyl with an unlabeled 20:4 acyl chain, leading to the formation of $^{13}\text{C}_{24}$ -PC16:0_20:4. Thus, the detection of both the lipid substrate and end products of this enzymatic-driven conversion provides the first direct observation of acyl remodeling events in tissue using MSI. Signal for $[\text{U}^{13}\text{C}\text{-DPPC}+\text{Na}]^+$ was absent from the bronchioles and distributed heterogeneously

throughout the parenchymal area. While this does not allow us to exclude the possibility of PC16:0/16:0 \rightarrow PC16:0_20:4 metabolism within the bronchioles, the observation of $[\text{U}^{13}\text{C}_{24}\text{-PC16:0_20:4}+\text{Na}]^+$ provides direct evidence for PC16:0/16:0 \rightarrow PC16:0_20:4 enzymatic synthesis within the lung parenchyma. The absence of $^{13}\text{C}_{24}$ -PC16:0_20:4 and U^{13}C -DPPC in the bronchial regions demonstrated the lack of surfactant uptake and PC metabolism by the bronchial epithelium. We found reasonable but not complete co-localization between

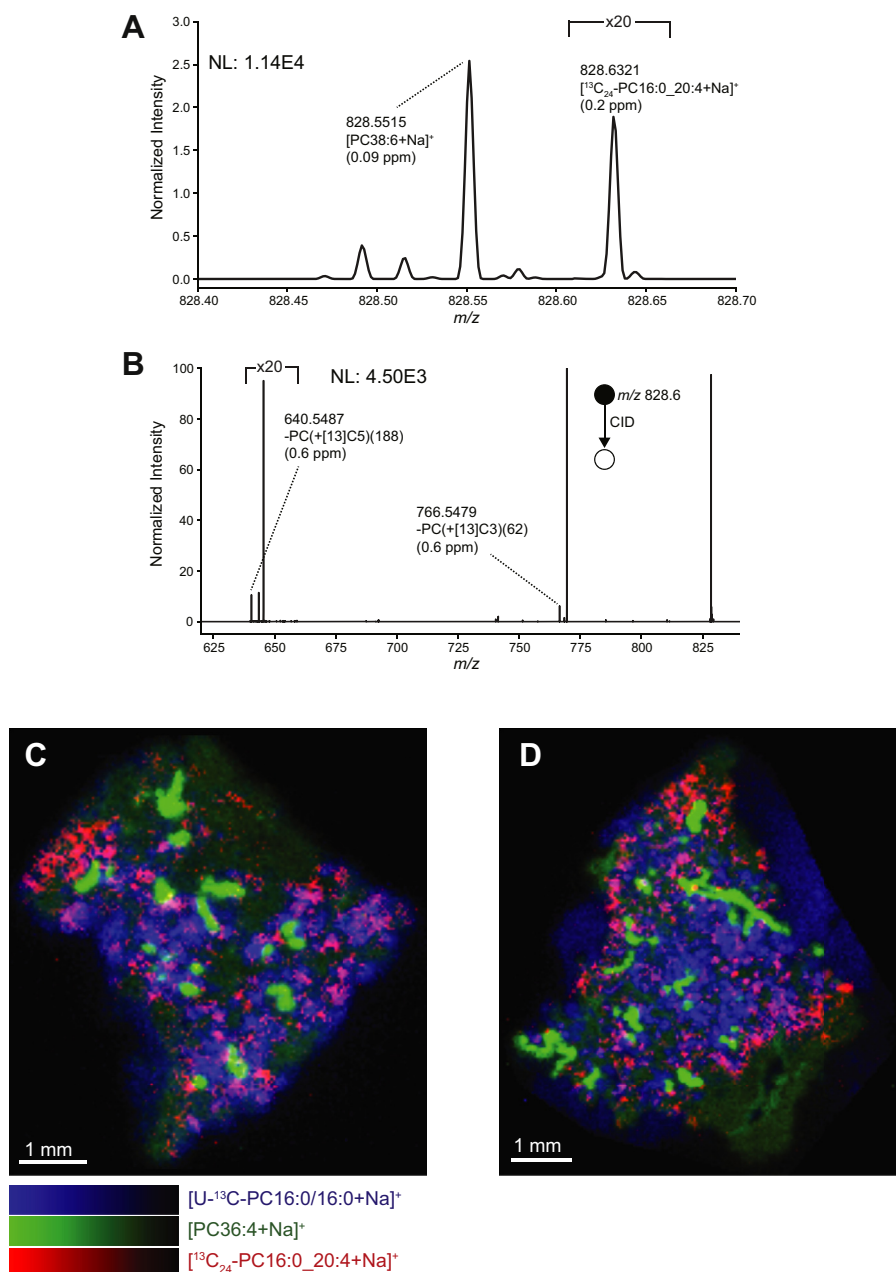


Fig. 6. MALDI-MSI of U¹³C-PC16:0/16:0 acyl chain remodeling. A: Averaged MALDI mass spectrum from lung tissue collected from mice euthanized 12 h after administration of D₉-choline and U¹³C-DPPC-containing Poractant alfa surfactant. The ion at *m/z* 828.6321 is assigned as the [M+Na]⁺ ion of ¹³C₂₄-PC16:0_20:4 formed by acyl remodeling of U¹³C-PC16:0/16:0. The “NL” value refers to the intensity of the base peak in the full range MS¹ spectrum. B: MS/MS spectrum of precursor ions at *m/z* 828.5 ± 0.5 with fragment ions originating from [¹³C₂₄-PC16:0_20:4+Na]⁺ annotated. Part-per-million (ppm) mass errors are provided in parentheses. C, D: MALDI-MSI data of [U¹³C-DPPC+Na]⁺ (blue), [PC36:4+Na]⁺ (green) and [¹³C₂₄-PC16:0_20:4+Na]⁺ (red) in lung tissue collected from mice (C) 12 h and (D) 18 h after label administration. All images were visualized using total-ion-current normalization and hotspot removal (high quantile = 99%). MS/MS, tandem mass spectrometry; MSI, mass spectrometry imaging; PC, phosphatidylcholine; U¹³C-DPPC, universally ¹³C-labeled dipalmitoyl PC.

¹³C₂₄-PC16:0_20:4 and U¹³C-DPPC, a perhaps not surprising observation as alveolar surfactant, and macrophages had been removed by lavage before the lungs were frozen. These distributions then presumably represent the patterns of cellular uptake of surfactant by ATII cells and macrophages as well as that of surfactant acyl remodeling in lung tissue-resident alveolar macrophages. Evidence for

the 22:6 acyl chain substitution on U¹³C-DPPC was observed but with insufficient signal for imaging. While the [¹³C₂₄-PC16:0_22:6+Na]⁺ ion was absent in the full-scan MSI data, MS/MS of expected precursor ion revealed a characteristic neutral loss of N(¹³CH₃)₃ (-PC(+¹³C3)(62)), thereby providing direct evidence for a [¹³C₂₄-PC16:0_22:6+Na]⁺ ion (supplemental Fig. S10). For enhanced sensitivity, this

MS/MS data were obtained following accumulation of precursor ions over a larger sample area before fragmentation and detection. The results thereby present evidence for the specific acyl remodeling of surfactant DPPC into polyunsaturated PC species by alveolar macrophages *in vivo*.

DISCUSSION


For the first time we have combined isotopic labeling with MALDI-MSI at high mass resolving power to visualize: (i) uptake and distribution of therapeutic surfactants used to treat a variety of respiratory diseases; and (ii) the location of lipid synthesis and metabolic events throughout biological tissue. Injection of D₉-choline into the mice enabled the detection and localization of newly synthesized PC lipids produced by the CDP:choline pathway by virtue of their expected *m/z* shift of 9.0654 (Δ_{9D-9H}). These metabolic events were found to be relatively homogeneously distributed throughout the mouse lung tissue. The use of a U¹³C-DPPC label not only enabled the visualization of both CHF5633 and Poractant alfa porcine surfactant uptake independent of endogenous surfactant but also allowed detection of acyl chain remodeling events within the tissue. In particular, de-acylation/re-acylation of U¹³C-DPPC via the Lands cycle was observed, forming ¹³C₂₄-PC16:0_20:4 within the parenchyma. We note that while it is often assumed that this process is initiated by PLA₂ cleavage of the *sn*-2 fatty acyl, analogous PLA₁ cleavage (31, 32), leading to the formation of ¹³C₂₄-PC20:4/16:0, is also possible. As a result, our approach not only provides lipid distributions, but the localization of lipid metabolic events within the tissue.

The metabolism of U¹³C-DPPC by alveolar macrophages *in vivo*, summarized in Fig. 5, provides strong circumstantial evidence for a major role for this cell type in the generation of ¹³C₂₄-PC16:0_20:4 by de-acylation/re-acylation of DPPC. While the active re-acylation of arachidonate into alveolar macrophage phospholipids has been reported previously (33, 34), the results presented here are the first demonstration of a similar re-acylation that is specific for docosahexaenoate. If re-acylation of arachidonate is indeed restricted to alveolar macrophages, this could explain the discrepancy of distribution of ¹³C₂₄-PC16:0_20:4 and U¹³C-DPPC shown in Fig. 6. This may possibly have been because of migration of alveolar macrophages within the lung parenchyma after initial uptake of the exogenous surfactant.

Surfactant catabolism and turnover have previously been studied both *in vivo* (35) and in isolated ATII cells (36) and alveolar macrophages (37), which are thought to be responsible for the turnover of surfactant phospholipid in healthy lung. However, there has been no demonstration of their relative contributions, as opposed to, for instance secretory phospholipase A₂

(38), to the decreased bronchoalveolar surfactant concentration in severe respiratory diseases such as acute respiratory distress syndrome. In contrast, the extensive accumulation of surfactant phospholipid and proteins in alveolar proteinosis is clearly because of impairment of granulocyte macrophage colony stimulating factor-dependent alveolar macrophage metabolism (39). MSI offers considerable potential to probe these mechanisms in increased detail, particularly as the sensitivity continues to improve, enabling the detection of even lower abundance labeled lipids and their metabolites (e.g., LPC species and D₃/D₆-labeled PC species that may form via metabolism of D₉-PC species). This detection sensitivity will be especially important if the relative roles of different individual cell types can be visualized, a possibility that is becoming feasible as current research aims to reduce the spatial resolution of MSI to the single-cell level (40, 41).

Data availability

Mass spectrometry imaging datasets in the open source imzML format are available for download from the MetaboLights repository (42) with study identifier MTBLS2075 (www.ebi.ac.uk/metabolights/MTBLS2075). 




Acknowledgements

This work was financially supported by the LINK program of the Dutch province of Limburg. S. R. E. acknowledges funding from the Australian Research Council Future Fellowship Scheme (grant number FT190100082) and the Netherlands Organisation for Scientific Research VIDI scheme (grant number 198.011). The authors are grateful to the NIHR Southampton Biomedical Research Centre for mass spectrometry support and to the Chiesi Farmaceutica for the supply of the therapeutic surfactants.

Author contributions

S. R. E., R. M. A. H., and A. D. P. conceived the project. S. R. E. and B. F. performed MSI sample preparation and data acquisition. H. W. C. and J. M. designed the mouse experiments and performed the mouse procedures; E. H. and M. P. performed the alveolar macrophage procedures; and G. K. and M. P. performed shotgun lipidomics experiments and analysed data. S. R. E. and A. D. P. analysed the MSI data. S. R. E., R. M. A. H., A. D. P., J. M., and H. W. C. financially supported the project. S. R. E. and A. D. P. wrote the paper with input from co-authors.

Author ORCIDs

Shane R. Ellis  <https://orcid.org/0000-0002-3326-5991>
Ron. M. A. Heeren  <https://orcid.org/0000-0002-6533-7179>
Anthony D. Postle  <https://orcid.org/0000-0001-7361-0756>

Conflict of interest

J. W. and H. W. C. received funding from the Chiesi Farmaceutica for the original study from which lung tissue

samples were provided for MSI. There are no other competing interests.

Abbreviations

ATII, Alveolar epithelial type II; BALF, Bronchoalveolar lavage fluid; CHCl₃, Chloroform; DPPC, Dipalmitoyl phosphatidylcholine; EtOH, Ethanol; MeOH, Methanol; MS/MS, Tandem mass spectrometry; MSI, Mass spectrometry imaging; PC, Phosphatidylcholine; PLA₁, Phospholipase A₁; PLA₂, Phospholipase A₂; SIMS, Secondary ion mass spectrometry.

Manuscript received October 26, 2020, and in revised form December 18, 2020. Published, JLR Papers in Press, January 14, 2021, <https://doi.org/10.1016/j.jlr.2021.100023>

REFERENCES

- Burdge, G. C., Kelly, F. J., and Postle, A. D. (1993) Synthesis of phosphatidylcholine in guinea-pig fetal lung involves acyl remodelling and differential turnover of individual molecular species. *Biochim. Biophys. Acta*. **1166**, 251–257
- Bridges, J. P., Ikegami, M., Brilli, L. L., Chen, X., Mason, R. J., and Shannon, J. M. (2010) LPCAT1 regulates surfactant phospholipid synthesis and is required for transitioning to air breathing in mice. *J. Clin. Invest.* **120**, 1736–1748
- Jain, D., Dodia, C., Fisher, A. B., and Bates, S. R. (2005) Pathways for clearance of surfactant protein A from the lung. *Am. J. Physiol. Lung Cell. Mol. Physiol.* **289**, L1011–L1018
- Gräbner, R., and Meerbach, W. (1991) Phagocytosis of surfactant by alveolar macrophages in vitro. *Am. J. Physiol. Lung Cell. Mol. Physiol.* **261**, L472–L477
- Wright, S. M., Hockey, P. M., Enhorning, G., Strong, P., Reid, K. B., Holgate, S. T., Djukanovic, R., and Postle, A. D. (2000) Altered airway surfactant phospholipid composition and reduced lung function in asthma. *J. Appl. Physiol.* **89**, 1283–1292
- Gross, N. J., Barnes, E., and Narine, K. R. (1988) Recycling of surfactant in black and beige mice, pool sizes and kinetics. *J. Appl. Physiol.* **64**, 2017–2025
- Wright, J. R. (1990) Clearance and recycling of pulmonary surfactant. *Am. J. Physiol.* **259**, L1–L12
- Bernhard, W., Pynn, C. J., Jaworski, A., Rau, G. A., Hohlfeld, J. M., Freihorst, J., Poets, C. F., Staud, D., and Postle, A. D. (2004) Mass spectrometric analysis of surfactant metabolism in human volunteers using deuterated choline. *Am. J. Respir. Crit. Care Med.* **170**, 54–58
- Postle, A. D., Henderson, N. G., Koster, G., Clark, H. W., and Hunt, A. N. (2011) Analysis of lung surfactant phosphatidylcholine metabolism in transgenic mice using stable isotopes. *Chem. Phys. Lipids*. **164**, 549–555
- Dushianthan, A., Goss, V., Cusack, R., Grocott, M. P., and Postle, A. D. (2014) Phospholipid composition and kinetics in different endobronchial fractions from healthy volunteers. *BMC Pulm. Med.* **14**, 10
- Dushianthan, A., Goss, V., Cusack, R., Grocott, M. P., and Postle, A. D. (2014) Altered molecular specificity of surfactant phosphatidylcholine synthesis in patients with acute respiratory distress syndrome. *Respir. Res.* **15**, 128
- Madsen, J., Panchal, M. H., Mackay, R. A., Echaide, M., Koster, G., Aquino, G., Pelizzi, N., Perez-Gil, J., Salomone, F., Clark, H. W., and Postle, A. D. (2018) Metabolism of a synthetic compared with a natural therapeutic pulmonary surfactant in adult mice. *J. Lipid Res.* **59**, 1880–1892
- Zemski Berry, K. A., Hankin, J. A., Barkley, R. M., Spraggins, J. M., Caprioli, R. M., and Murphy, R. C. (2011) MALDI imaging of lipid biochemistry in tissues by mass spectrometry. *Chem. Rev.* **111**, 6491–6512
- Bowman, A. P., Heeren, R. M. A., and Ellis, S. R. (2019) Advances in mass spectrometry imaging enabling observation of localised lipid biochemistry within tissues. *TrAC Trends Anal. Chem.* **120**, 115197
- Berry, K. A., Li, B., Reynolds, S. D., Barkley, R. M., Gijon, M. A., Hankin, J. A., Henson, P. M., and Murphy, R. C. (2011) MALDI imaging MS of phospholipids in the mouse lung. *J. Lipid Res.* **52**, 1551–1560
- Jacobs, E. R., and Zeldin, D. C. (2001) The lung HETEs (and EETs) up. *Am. J. Physiol. Heart Circ. Physiol.* **280**, H1–H10
- Calabrese, C., Triggiani, M., Marone, G., and Mazzarella, G. (2000) Arachidonic acid metabolism in inflammatory cells of patients with bronchial asthma. *Allergy*. **55**, 27–30
- Frisz, J. F., Lou, K., Klitzing, H. A., Hanafin, W. P., Lizunov, V., Wilson, R. L., Carpenter, K. J., Kim, R., Hutcheon, I. D., Zimmerberg, J., Weber, P. K., and Kraft, M. L. (2013) Direct chemical evidence for sphingolipid domains in the plasma membranes of fibroblasts. *Proc. Natl. Acad. Sci. U. S. A.* **110**, E613–E622
- Jiang, H., Goulbourne, C. N., Tatar, A., Turlo, K., Wu, D., Beigneux, A. P., Grovenor, C. R. M., Fong, L. G., and Young, S. G. (2014) High-resolution imaging of dietary lipids in cells and tissues by NanoSIMS analysis. *J. Lipid Res.* **55**, 2156–2166
- Arts, M., Soons, Z., Ellis, S. R., Pierzchalski, K. A., Balluff, B., Eijkel, G. B., Dubois, L. J., Lieuwes, N. G., Agten, S. M., Hackeng, T. M., van Loon, L. J. C., Heeren, R. M. A., and Olde Damink, S. W. M. (2017) Detection of localized hepatocellular amino acid kinetics by using mass spectrometry imaging of stable isotopes. *Angew. Chem. Int. Ed. Engl.* **56**, 7146–7150
- Carson, R. H., Lewis, C. R., Erickson, M. N., Zagieboylo, A. P., Naylor, B. C., Li, K. W., Farnsworth, P. B., and Price, J. C. (2017) Imaging regioselective lipid turnover in mouse brain with desorption electrospray ionisation mass spectrometry. *J. Lipid Res.* **58**, 1884–1892
- Bligh, E. G., and Dyer, W. J. (1959) A rapid and sensitive method of total lipid extraction and purification. *Can. J. Biochem. Physiol.* **37**, 911–917
- Belov, M. E., Ellis, S. R., Dilillo, M., Paine, M. R. L., Danielson, W. F., Anderson, G. A., de Graaf, E. L., Eijkel, G. B., Heeren, R. M. A., and McDonnell, L. A. (2017) Design and performance of a novel interface for combined matrix-assisted laser desorption ionization at elevated pressure and electrospray ionization with orbitrap mass spectrometry. *Anal. Chem.* **89**, 7493–7501
- Tortorella, S., Tiberi, P., Bowman, A. P., Claes, B. S. R., Ščupáková, K., Heeren, R. M. A., Ellis, S. R., and Cruciani, G. (2020) LipostarMSI: comprehensive, vendor-neutral software for visualization, data analysis, and automated molecular identification in mass spectrometry imaging. *J. Am. Soc. Mass. Spectrom.* **31**, 155–163
- Pauling, J. K., Hermansson, M., Hartler, J., Christiansen, K., Gallego, S. F., Peng, B., Ahrends, R., and Ejsing, C. S. (2017) Proposal for a common nomenclature for fragment ions in mass spectra of lipids. *PLoS One*. **12**, e0188394
- Kennedy, E. P., and Weiss, S. B. (1956) The function of cytidine coenzymes in the biosynthesis of phospholipides. *J. Biol. Chem.* **222**, 193–214
- Goss, V., Hunt, A. N., and Postle, A. D. (2013) Regulation of lung surfactant phospholipid synthesis and metabolism. *Biochim. Biophys. Acta. Mol. Cell. Biol. Lipids*. **1831**, 448–458
- Lands, W. E. M. (2000) Stories about acyl chains. *Biochim. Biophys. Acta*. **1483**, 1–14
- Shindou, H., and Shimizu, T. (2009) Acyl-CoA:Lysophospholipid Acyltransferases. *J. Biol. Chem.* **284**, 1–5
- Nakagawa, Y., and Waku, K. (1986) Synthesis of the dipalmitoyl species of diacyl glycerophosphocholine by rabbit alveolar macrophages. *Lipids*. **21**, 155–158
- Heath, M. F., and Jacobson, W. (1976) Phospholipases A₁ and A₂ in lamellar inclusion bodies of the alveolar epithelium of rabbit lung. *Biochim. Biophys. Acta*. **441**, 443–452
- Rao, R. H., Waite, M., and Myrvik, Q. N. (1981) Deacylation of dipalmitoyllecithin by phospholipases A in alveolar macrophages. *Exp. Lung Res.* **2**, 9–15
- Cochran, F. R., Roddick, V. L., Connor, J. R., Thornburg, J. T., and Waite, M. (1987) Regulation of arachidonic acid metabolism in resident and BCG-activated alveolar macrophages: role of lyso(bis)phosphatidic acid. *J. Immunol.* **138**, 1877–1883
- Ralston, N. V., Schmid, P. C., and Schmid, H. H. (1998) Agonist-stimulated glycerophospholipid acyl turnover in alveolar macrophages. *Biochim. Biophys. Acta*. **1393**, 211–221
- Ikegami, M. (2006) Surfactant catabolism. *Respirology*. **11 Suppl**, S24–S27
- Griese, M., Beck, J., and Feuerhake, F. (1999) Surfactant lipid uptake and metabolism by neonatal and adult type II pneumocytes. *Am. J. Physiol.* **277**, L901–L909
- Wright, J. R., and Youmans, D. C. (1995) Degradation of surfactant lipids and surfactant protein A by alveolar macrophages in vitro. *Am. J. Physiol.* **268**, L772–L780

38. Arbibe, L., Koumanov, K., Vial, D., Rougeot, C., Faure, G., Havet, N., Longacre, S., Vargaftig, B. B., Béréziat, G., Voelker, D. R., Wolf, C., and Touqui, L. (1998) Generation of lyso-phospholipids from surfactant in acute lung injury is mediated by type-II phospholipase A2 and inhibited by a direct surfactant protein A-phospholipase A2 protein interaction. *J. Clin. Invest.* **102**, 1152–1160
39. Carey, B., and Trapnell, B. C. (2010) The molecular basis of pulmonary alveolar proteinosis. *Clin. Immunol.* **135**, 223–235
40. Kompauer, M., Heiles, S., and Spengler, B. (2017) Atmospheric pressure MALDI mass spectrometry imaging of tissues and cells at 1.4- μm lateral resolution. *Nat. Methods.* **14**, 90–96
41. Niehaus, M., Soltwisch, J., Belov, M. E., and Dreisewerd, K. (2019) Transmission-mode MALDI-2 mass spectrometry imaging of cells and tissues at subcellular resolution. *Nat. Methods.* **16**, 925–931
42. Haug, K., Cochrane, K., Nainala, V. C., Williams, M., Chang, J., Jayaseelan, K. V., and O'Donovan, C. (2019) MetaboLights: a resource evolving in response to the needs of its scientific community. *Nucleic Acids Res.* **48**, D440–D444